AGU PUBLICATIONS

Geophysical Research Letters

RESEARCH LETTER
10.1002/2016GL070058

Key Points:
- Southern Ocean surface forcing controls the global deep ocean density stratification over a larger depth range than previously thought
- Fixed Southern Ocean surface buoyancy fluxes rather than fixed surface density controls the deep density stratification
- But the temperature and salinity components of the deep stratification are strongly influenced by Northern Hemisphere surface forcing

Supporting Information:
- Supporting Information S1

Correspondence to:
S. Sun,
shantong@ucsd.edu

Citation:
Sun, S., I. Eisenman, and A. Stewart (2016), The influence of Southern Ocean surface buoyancy forcing on glacial-interglacial changes in the global deep ocean stratification, *Geophys. Res. Lett.*, *43*, 8124–8132, doi:10.1002/2016GL070058.

Received 17 JUN 2016
Accepted 14 JUL 2016
Accepted article online 21 JUL 2016
Published online 4 AUG 2016

The influence of Southern Ocean surface buoyancy forcing on glacial-interglacial changes in the global deep ocean stratification

S. Sun[1], I. Eisenman[1], and A. L. Stewart[2]

[1]Scripps Institution of Oceanography, University of California, San Diego, La Jolla, USA, [2]Department of Atmospheric and Oceanic Sciences, University of California, Los Angeles, USA

Abstract Previous studies have suggested that the global ocean density stratification below ~3000 m is approximately set by its direct connection to the Southern Ocean surface density, which in turn is constrained by the atmosphere. Here the role of Southern Ocean surface forcing in glacial-interglacial stratification changes is investigated using a comprehensive climate model and an idealized conceptual model. Southern Ocean surface forcing is found to control the global deep ocean stratification up to ~2000 m, which is much shallower than previously thought and contrary to the expectation that the North Atlantic surface forcing should strongly influence the ocean at intermediate depths. We show that this is due to the approximately fixed surface freshwater fluxes, rather than a fixed surface density distribution in the Southern Ocean as was previously assumed. These results suggest that Southern Ocean surface freshwater forcing controls glacial-interglacial stratification changes in much of the deep ocean.

1. Introduction

During the Last Glacial Maximum (LGM), the climate was characterized by a colder global-mean temperature and lower atmospheric CO_2 concentration compared with today [e.g., *Clark et al.*, 2009]. An enhanced stratification of the deep ocean (below ~1000 m depth) has been proposed as a key contributor to the lower atmospheric CO_2 concentration at the LGM by acting as a more effective carbon trap [*Bouttes et al.*, 2009; *Adkins*, 2013]. The deep ocean stratification also influences the strength of the abyssal overturning circulation, which has been invoked to explain reduced CO_2 outgassing and hence a lower CO_2 concentration at the LGM [*Sarmiento and Toggweiler*, 1984; *Anderson et al.*, 2009; *Sigman et al.*, 2010].

As a large-scale feature that is closely tied to the global ocean overturning circulation, the processes that maintain the stratification of the deep ocean (including both abyssal and middepth regions) have attracted substantial attention for many years. Studies by *Munk* [1966] and *Munk and Wunsch* [1998] proposed that the deep stratification and overturning circulation are controlled to first order by a balance between the vertical advection and diffusion of buoyancy. More recent studies have suggested that Southern Ocean processes play a key role in closing the global overturning circulation and setting the deep ocean stratification [*Marshall and Speer*, 2012; *Wolfe and Cessi*, 2010].

Nikurashin and Vallis [2011, 2012] combined these ideas in a conceptual model, in which the surface density was specified in the Southern Ocean. In this model, the abyssal stratification associated with the abyssal overturning circulation, i.e., the lower cell that spreads Antarctic Bottom Water (AABW) throughout the global ocean below ~3000 m, is essentially set by the Southern Ocean surface density profile with some modulation by the competing wind-driven and eddy-driven overturning circulations in the Southern Ocean.

Above the abyssal overturning circulation and below the main thermocline (typically from 3000 m to 1000 m depth in the Atlantic Ocean), diapycnal mixing is relatively weak [*Kunze et al.*, 2006]. The stratification in this middepth region is associated with the nearly adiabatic pole-to-pole overturning circulation (i.e., the upper cell) [*Wolfe and Cessi*, 2011] that spreads North Atlantic Deep Water (NADW) southward from the North Atlantic and spreads Antarctic Intermediate Water (AAIW) northward from the Southern Ocean [*Talley*, 2013; *Lozier*, 2012]. The stratification at this depth is modulated by surface buoyancy and momentum forcing conditions in both the Southern Ocean and the North Atlantic [*Wolfe and Cessi*, 2011].

Though these idealized modeling studies are conceptually illuminating, the applicability of their predictions to the real ocean is limited. Most of these studies employ an idealized topography, a single ocean basin, and a single thermodynamic variable (rather than including both temperature and salinity), which leads to an overturning circulation that is split into two isolated cells [e.g., *Wolfe and Cessi*, 2010, 2011; *Munday et al.*, 2013]. However, a property-based reconstruction of the overturning circulation suggests that the upper and lower cells are in fact actively coupled and follow a three-dimensional pathway through all of the major ocean basins [*Talley*, 2013]. Additionally, idealized modeling studies typically employ restoring to a fixed buoyancy profile over a prescribed time scale at the ocean surface, which may not accurately reflect the surface buoyancy fluxes in regions where they are dominated by freshwater fluxes, such as the Southern Ocean [*Cerovecki et al.*, 2011; *Stewart et al.*, 2014].

The present study is the first (as far as the authors are aware) to investigate the influence of the Southern Ocean surface forcing on the global deep ocean stratification in the relatively realistic setting of a comprehensive climate model. In section 2, we describe the experimental setup, which consists of three ocean-only climate model simulations that are designed to isolate the influence of the Southern Ocean surface forcing on the changes in the global deep ocean stratification between the LGM and the preindustrial (PI) climate. In section 3, we present the model simulation results and discuss the relative roles of the Southern Ocean and the Northern Hemisphere surface forcing in setting the global deep ocean stratification. In section 4, we use a conceptual model to interpret the results from the climate model simulations. Concluding remarks are provided in section 5.

2. Experimental Design

We use a state-of-the-art climate model, the National Center for Atmospheric Research (NCAR) Community Earth System Model version 1.1.2 (CESM1.1.2), which we run in a configuration with only the ocean component active and the atmosphere, sea ice, and land runoff specified from two previous coupled simulations. One coupled simulation represents the PI climate [*Gent et al.*, 2011], and the other coupled simulation represents the LGM climate [*Brady et al.*, 2013]. Further information about the model setup and forcing is included in the supporting information.

We perform three experiments that share the same model configuration (including the same PI ocean bathymetry) but have different ocean surface forcing: one control run (PI) is forced by PI surface conditions, a second control run (LGM) is forced by LGM surface conditions, and a test run (Test) is forced by LGM surface conditions in the Southern Ocean and PI surface conditions elsewhere. More precisely,

$$F_{\mathrm{Test}} = \gamma F_{\mathrm{PI}} + (1-\gamma) F_{\mathrm{LGM}},$$

where γ is 0 to the south of 40°S, 1 to the north of 30°S, and increases linearly from 0 to 1 between 40°S and 30°S. Here F_{PI} and F_{LGM} denote the surface forcing fields derived from the PI and LGM coupled runs, respectively, and F_{Test} denotes the surface forcing fields used for the Test run (see supporting information for further details). In each case, the coupled model output is used to construct surface forcing fields that repeat every 30 years.

All three runs are initialized from the same initial conditions obtained from the PI coupled run. The length of each integration is listed in Table S1 of the supporting information along with the trend during the last 120 years of the global volume-average temperature, ideal age, and Atlantic Meridional Overturning Circulation (AMOC) maximum (defined as the maximum total overturning circulation streamfunction below 500 m in the Atlantic Ocean including contributions from both the mean flow and the parameterized eddies). Although the trends are nonzero, Table S1 indicates that all three runs are close to equilibration (see also supporting information Figures S3 and S6). Note that all simulations are initiated from the PI coupled run, so the PI ocean-only run equilibrates more rapidly than the Test and LGM runs. Unless otherwise noted, the results presented in this study are averaged over the last 20 years of each model run.

Figure 1 shows the zonal-mean surface buoyancy flux (B) in each simulation, along with its heat (B_{HF}) and freshwater (B_{FW}) components defined as

$$B = B_{\mathrm{HF}} + B_{\mathrm{FW}} \equiv \alpha g \frac{Q_{\mathrm{HF}}}{c_p \rho_0} + \beta S g Q_{\mathrm{FW}}, \quad (1)$$

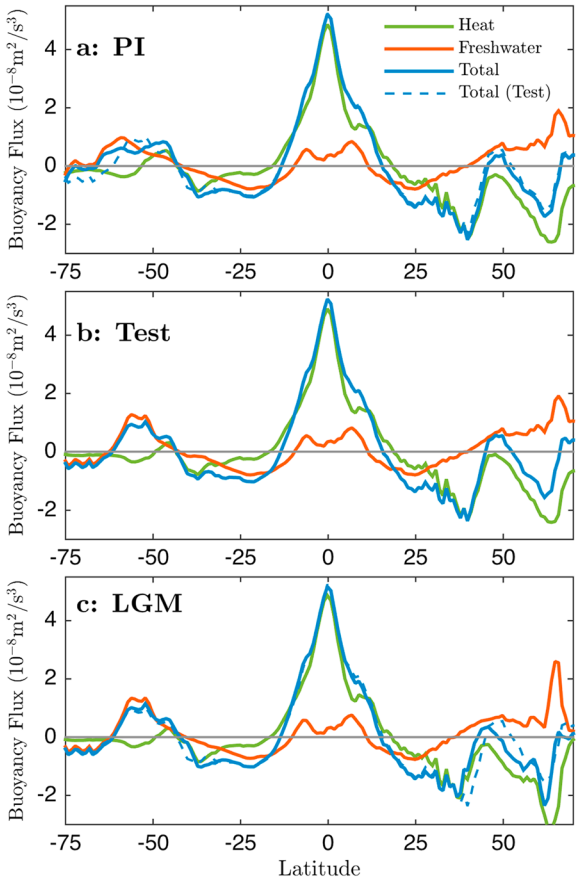

Figure 1. (a–c) Zonal-mean surface buoyancy flux for the three model runs along with its heat and freshwater components. The total buoyancy flux from the Test run is plotted for comparison in Figures 1a and 1c as a blue dashed line.

where g is the gravitational acceleration, ρ_0 is a reference density, c_p is the specific heat of seawater, S is the ocean surface salinity, α is the thermal expansion coefficient, β is the saline contraction coefficient, Q_{HF} is the net air-sea heat flux (positive for ocean heat gain), and Q_{FW} is the net freshwater flux (positive for ocean freshwater gain). The freshwater flux is approximately fixed by the prescribed forcing in each run. It is mainly associated with sea ice melting and freezing, river runoff, precipitation, and evaporation, and all but the last of these fields are fully specified in the simulations. The surface heat flux in these simulations, on the other hand, more closely resembles a restoring boundary condition [cf. *Haney*, 1971]. The freshwater flux does include a "weak restoring" component to avoid unbounded local salinity trends under mixed boundary conditions [*Griffies et al.*, 2009], but this component does not appear to substantially influence the results presented here, as discussed in the supporting information. Figure 1 shows that south of 45°S, the buoyancy flux is mostly dominated by the freshwater flux, implying that the Southern Ocean is subject to a surface buoyancy flux that is approximately fixed, i.e., independent of ocean state.

Note that the form of the surface buoyancy flux (restoring boundary condition or fixed buoyancy flux) has been shown to strongly influence the response of the deep ocean to surface forcing perturbations. In an eddy-resolving channel model, *Abernathey et al.* [2011] found different sensitivities of the overturning circulation to surface wind stress between simulations with fixed buoyancy flux and those with restoring boundary conditions, as was similarly found in a conceptual model by *Stewart et al.* [2014].

3. CESM Simulation Results

3.1. Stratification and Overturning Circulation

We first discuss the mean stratification and overturning circulation in the Test simulation, introducing a conceptual decomposition of the domain into three dynamically distinct regions in order to facilitate interpretation of the results. We focus our analysis on the Atlantic basin because, due to the formation of the NADW, the Northern Hemisphere surface forcing is expected to have more influence on the deep ocean stratification in the Atlantic basin than in the Pacific and Indian basins. A meridional section of σ_2 (i.e., potential density referenced to 2000 dbar) that is zonally averaged between 25°W and 35°W in the Test run is presented in Figure 2b, with the residual overturning circulation streamfunction in the Atlantic Ocean included as black contours.

By comparing the overturning circulation streamfunction to the potential density, we identify three distinct isopycnal regions in the Atlantic Basin which are separated by isopycnal surfaces ρ_1 and ρ_2. This is shown schematically in Figure 2c. Here ρ_2 is defined as the density of the isopycnal that separates the upper and lower overturning circulation cells. As shown in Figure 2a, it also coincides with the border between the regions of

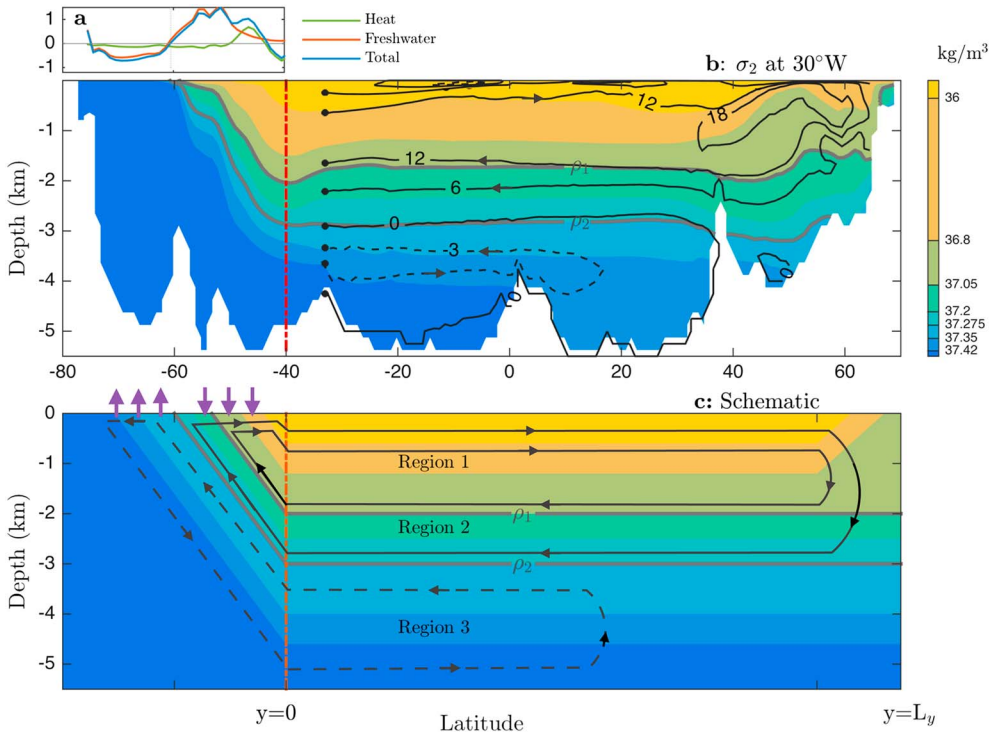

Figure 2. (a) Buoyancy forcing averaged between 25°W and 35°W in the Southern Ocean in the Test run, plotted in units of 10^{-8} m^2/s^3. (b) Meridional section of σ_2 (shading) from the Test run, averaged zonally between 25°W and 35°W. The residual overturning circulation streamfunction in the Atlantic Ocean, calculated on σ_2 surfaces and then mapped back to depth coordinates, is included as black contours with arrows indicating the direction of flow. (c) Schematic of the isopycnals (shading) and overturning circulation (black lines with arrows). Purple arrows in the Southern Ocean indicate the direction of buoyancy flux, with ocean buoyancy loss indicated by upward arrows. The northern boundary of the Antarctic Circumpolar Current (ACC) is indicated in panels b and c by a red dash dotted line. The thick gray lines represent the isopycnals that separate these 3 regions (ρ_1 and ρ_2). Here ρ_2 is defined as the density of the isopycnal surface that separates the upper and lower overturning circulation cells, and ρ_1 is defined more approximately as the density of the isopycnal below which the isopycnal surfaces are approximately flat and hence are not substantially affected by the near-surface wind-driven circulation.

buoyancy loss and gain in the Southern Ocean in the long-term mean, which is approximately 10° south of the westerly wind maximum in the Atlantic Sector of the Southern Ocean. We define ρ_1 as the uppermost isopycnal surface that outcrops in the Southern Ocean but not in the Northern Hemisphere in the long-term mean. Below ρ_1, the isopycnal surfaces are nearly flat in Figure 2b, implying that they are not substantially affected by the surface wind-driven circulation.

In Region 3, isopycnals outcrop only in regions in the Southern Ocean where the ocean loses buoyancy at the surface (Figure 2b). Region 3 coincides with the depths spanned by the counterclockwise lower overturning circulation cell (ψ<0). In Region 2, which represents the middepth ocean, isopycnals outcrop only in regions in the Southern Ocean where the ocean gains buoyancy in the long-term mean (Figure 2b), although they occasionally outcrop in the high-latitude North Atlantic during the winter season. In both Region 2 and Region 3, isopycnals are approximately flat except in the Southern Ocean, and hence, they do not appear to be affected by the wind-driven circulation except in the Southern Ocean.

Region 1 spans from the top of Region 2 to the surface. Here isopycnals outcrop in both the Southern Ocean and the high-latitude North Atlantic in the long-term mean, and the influence of the wind-driven circulation becomes apparent particularly in the subpolar gyre of the North Atlantic (40–60°N). In the PI and LGM model runs, we identify analogous regions and adjust the potential densities ρ_1 and ρ_2 to match the isopycnals that separate them (see Figure S8 for the PI and LGM).

3.2. Role of Southern Ocean Surface Forcing

We now compare the basin-average stratification in the Atlantic basin between 20°S and 20°N. The result is presented in Figure 3 as the squared Brunt-Väisälä frequency N^2, which is reported in CESM as $N^2 \equiv -\frac{g}{\rho_0}\frac{\partial \sigma_{\mathrm{Pr}}}{\partial z}$,

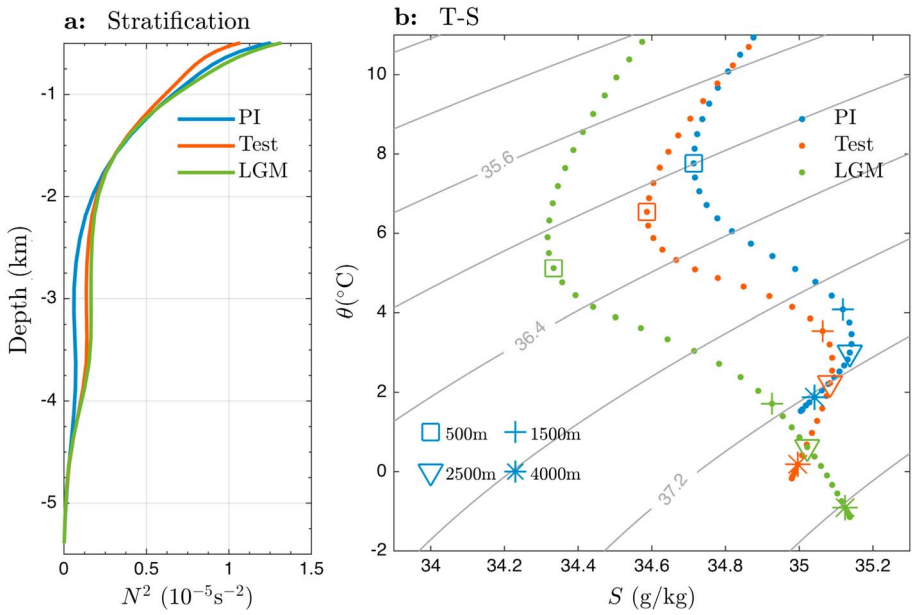

Figure 3. (a) Stratification (represented by the squared Brunt-Väisälä frequency N^2) averaged laterally between 20°S and 20°N in the Atlantic Ocean. (b) Temperature-salinity diagram for the three runs averaged between 20°S and 20°N in the Atlantic Ocean. Contours of σ_2 are indicated. The differences in σ_2 between 500 m and 1500 m are 0.99, 0.89, and 1.01 kg/m^3 in the PI, Test, and LGM runs, respectively; the differences between 2500 and 4000 m are 0.09, 0.20, and 0.27 kg/m^3, respectively.

where σ_{p_r} is the potential density referenced to the local pressure. The Test run closely reproduces the deep ocean stratification of the LGM run below approximately 2000 m, but not between 500 m and 1500 m. This indicates that the influence of the Southern Ocean on the deep stratification extends much higher in depth level than previously thought [e.g., *Nikurashin and Vallis*, 2012], approximately 1000 m above the boundary between the upper and lower overturning cells in the Atlantic. The stratification in the other major ocean basins largely supports this conclusion, suggesting that the surface forcing in the Southern Ocean is responsible for the enhanced global deep ocean stratification during the LGM in CESM (see supporting information for details).

Next, we examine the thermal and haline components of the deep ocean density stratification. Figure 3b shows a temperature-salinity (T-S) diagram, averaged laterally over the Atlantic basin between 20°S and 20°N. This figure indicates that the density difference between 2500 m (triangles) and 4000 m (stars) is much smaller in the PI run than in the Test and LGM runs, consistent with Figure 3a. However, the deep ocean temperature and salinity stratification in the Test run are strikingly different from the LGM run, having a negative rather than positive deep salinity stratification that more closely resembles the PI run. Though the density stratification is more dynamically relevant, the temperature and salinity stratifications are also important because they influence the stored heat and solubility of the abyssal waters, thereby affecting the capacity for carbon storage in the ocean.

Hence, Figure 3 implies that although North Atlantic surface forcing does not substantially affect the deep ocean density stratification, it does strongly influence the global deep ocean temperature and salinity profiles. This occurs in such a way that the deep ocean temperature and salinity differences between the simulations have canceling contributions to the deep ocean density stratification. This may be because both isopycnal advection and diffusion can influence the temperature and salinity along isopycnals between the Southern Ocean surface and the abyssal ocean, whereas the deep ocean density stratification is constrained by the Southern Ocean surface forcing. Consequently, there is a degree of freedom in how temperature and salinity vary with depth in the deep ocean.

4. Conceptual Model

Previous idealized studies [e.g., *Nikurashin and Vallis*, 2012] suggested that the density stratification in what we identify as Region 3 is constrained by the surface buoyancy forcing in the Southern Ocean. This is because surface buoyancy restoring essentially fixes the density gradient at the surface, and the approximately constant isopycnal slope in the Southern Ocean maps this surface density gradient to the abyssal ocean density stratification. In Region 2, however, they suggested that the stratification is substantially influenced by North Atlantic surface forcing as well, in contrast with the result presented in section 3.

In this section we adapt the zonally integrated conceptual model of *Nikurashin and Vallis* [2011] to investigate why the stratification in Region 2 in the CESM simulations appears to be largely controlled by the Southern Ocean alone. As discussed below, we find that the approximately fixed surface buoyancy flux in the Southern Ocean exerts a strong control over the density stratification in both Region 3 and Region 2, even though Region 2 contains the southward flow of the NADW.

As derived in the supporting information Text S3.i, the deep ocean stratification (N^2) can be related to the Southern Ocean surface buoyancy forcing in the conceptual model via a buoyancy budget equation:

$$\frac{\kappa L_x L_y}{N^2(z)} \frac{\partial}{\partial z} N^2(z) = \psi^*(z) + L_x \frac{B(-z/s)}{s\, N^2(z)}. \tag{2}$$

This states that the net diffusively driven upwelling across a given depth (or isopycnal surface) in the interior basin (left-hand side of equation (2)) is equal to the net export of NADW below that depth at the northern end of the basin (ψ^*) plus the net transformation from lighter to denser water at the Southern Ocean surface due to the zonal-mean surface buoyancy flux (B). Here κ is the diapycnal diffusivity, L_y and L_x are the meridional and zonal length scales of the basin (as in Figure 2b), ψ^* is the residual overturning circulation streamfunction at the northern boundary of the basin (i.e., at $y = L_y$), and s is the isopycnal slope in the Southern Ocean. Note that positive values of B here correspond to positive buoyancy input to the ocean and that the isopycnal slope (s) is negative.

Motivated by Figure 1, we model the surface buoyancy forcing as a fixed flux that varies with latitude, $B = B(y)$. In equation (2), B is evaluated at the location at which an isopycnal lying at depth z north of the Southern Ocean outcrops at the Southern Ocean surface, $y = -z/s$ (cf. Figure 2c). In order to simplify the conceptual model, we assume that both κ and s are constant. We find that s is approximately identical among the three simulations discussed above [cf. *Gent and Danabasoglu*, 2011], which is consistent with the assumption of constant isopycnal slope in the conceptual model. In supporting information Text S3.ii, we present a more general analysis that allows the isopycnal slope to change in response to the strength of overturning circulation. Note that the depth dependence of κ has been shown to be important for aspects of the deep ocean stratification, especially close to the depth of bottom topography [*Mashayek et al.*, 2015].

Region 3 is defined to lie below the southward flow of NADW, so ψ^* vanishes in this region (see Figure S8). Equation (2) in Region 3 thus can be written as

$$\frac{\partial}{\partial z} N^2(z) = \frac{B(-z/s)}{\kappa\, s\, L_y}. \tag{3}$$

Figure 3a shows that the stratification at the ocean bottom (N^2_{bot}) is close to zero in all three simulations, i.e., $N^2_{\mathrm{bot}} \approx 0$. Therefore, the stratification N^2 at any depth z within Region 3 is equal to the vertical integral of the right-hand side of equation (3) from the ocean bottom up to that depth, and hence, it is solely determined by the Southern Ocean surface buoyancy forcing. Because $B_{\mathrm{LGM}} \approx B_{\mathrm{Test}}$ in Figure 1c, it follows that $N^2_{\mathrm{LGM}} \approx N^2_{\mathrm{Test}}$ throughout Region 3 in Figure 3, where the subscripts indicate the model run. It should be noted that this is true only because the buoyancy forcing takes the form of a fixed flux in equation (2): if a relaxation boundary condition were applied as in previous idealized modeling studies [e.g., *Wolfe and Cessi*, 2011; *Nikurashin and Vallis*, 2012], then the stratification in Region 3 would be at least slightly impacted by interhemispheric effects, as shown by *Fučkar and Vallis* [2007] and in equation (S7) in the supporting information.

This argument does not extend to Region 2, because the southward flow of NADW is nonzero there, so the ψ^* term in equation (2) does not vanish. Instead, it can be shown that in order to produce a substantial difference

between the Test and LGM stratification in Region 2, a very large change in ψ^* would be required, which is much larger than the difference in ψ^* between the LGM and PI simulations. Rearranging equation (2) and taking the difference between the LGM and Test simulations, we obtain

$$\kappa L_y L_x \frac{\partial}{\partial z}\left(N^2_{\mathrm{LGM}}(z) - N^2_{\mathrm{Test}}(z)\right) = N^2_{\mathrm{LGM}}(z)\psi^*_{\mathrm{LGM}}(z) - N^2_{\mathrm{Test}}(z)\psi^*_{\mathrm{Test}}(z) \tag{4}$$

in Region 2. Here we have neglected the difference between the Test and LGM fixed surface buoyancy fluxes in the Southern Ocean, $B_{\mathrm{LGM}} - B_{\mathrm{Test}}$, because Figure 1c shows this term to be small.

At the boundary between Region 2 and Region 3 (~3000 m depth), Figure 3a indicates that the stratification at this depth is approximately equivalent between the LGM and Test simulations, i.e., $\Delta N^2 \equiv N^2_{\mathrm{LGM}} - N^2_{\mathrm{Test}} \approx 0$. Qualitatively, in order for the terms on the right-hand side of equation (4) to produce a vertical change in ΔN^2 of order N^2, the difference between the NADW transports $\left(\Delta\psi^* \equiv \psi^*_{\mathrm{LGM}} - \psi^*_{\mathrm{Test}}\right)$ in Region 2 must be large. Scaling arguments suggest that this requires $\Delta\psi^* \sim \kappa L_y L_x / H_2$, where $H_2 \approx 1000$ m is the vertical thickness of Region 2 (see supporting information for details). For typical oceanic parameter values, this requires a change in the NADW transport streamfunction $\Delta\psi^*$ of $\mathcal{O}$(10 sverdrup (Sv)). However, the strength of the streamfunction in this region is less than 10 Sv in the LGM and Test simulations, with the difference between the two being only $\Delta\psi^* \sim 2$ Sv. Thus, in the absence of extreme perturbations to the high-latitude Northern Hemisphere surface forcing, the Southern Ocean essentially controls the stratification throughout Region 2, consistent with the CESM result (Figure 3). This is also true when we relax the assumption of constant isopycnal slope (see supporting information Text S3.ii).

In Region 1, where the isopycnals outcrop in both the Southern Ocean and the North Atlantic, the ocean stratification is expected to be affected by a variety of processes, including the wind-driven gyre circulation and surface forcing in the high northern and southern latitudes [*Wolfe and Cessi*, 2011].

Conceptually, the analysis above suggests that the stratification in Region 3 is constrained by the requirement that all buoyancy loss by density classes at the surface in the Southern Ocean south of the outcrop position of ρ_2 must be balanced outside of the Southern Ocean by the net interior diffusive buoyancy flux across ρ_2. This argument can almost be extended to Region 2, except that the injection of NADW also contributes to the buoyancy budget in this region. However, because the southward NADW transport in Region 2 needs to change by much more than it does between the LGM and PI runs to substantially impact the stratification, this contribution from NADW can thus be thought of as essentially constant. Consequently, the surface buoyancy flux in the Southern Ocean provides a strong control of the stratification up to ~2000 m depth, as the CESM simulations indicate. This stands in contrast with previous idealized modeling studies [e.g., *Nikurashin and Vallis*, 2012; *Wolfe and Cessi*, 2011], where the stratification in the depth range that we identify as Region 2 is affected by the Northern Hemisphere surface forcing as well.

We emphasize that this conceptual model provides only an approximate qualitative picture of the effect of Southern Ocean surface buoyancy forcing on the global deep ocean stratification. The simplifications involved in the conceptual model make it difficult to find direct quantitative points of contact with the CESM simulations. For example, as shown in Figures S4 and S5 of the supporting information, the stratification profiles in the Pacific and Indian Oceans look different from the Atlantic. Understanding of this difference would require knowledge of the three-dimensional global overturning circulation, which is not included in the zonal-mean representation of the conceptual model.

5. Summary

The CESM ocean-only simulations presented here suggest that surface buoyancy forcing in the Southern Ocean largely controls the response of the abyssal stratification to LGM conditions. This is superficially consistent with previous understanding [*Nikurashin and Vallis*, 2011, 2012]. However, we furthermore find that this control extends up to approximately 2000 m depth, which is close to the core of the upper overturning circulation cell in the Atlantic. This is much shallower than expectations based on previous idealized modeling studies, which found the stratification above the abyssal ocean (i.e., in the middepth) to be substantially affected by North Atlantic surface forcing [e.g., *Nikurashin and Vallis*, 2012; *Wolfe and Cessi*, 2011]. We interpret the simulation results using a zonally integrated conceptual model. The analysis suggests that the control of the Southern Ocean surface buoyancy forcing over the global deep ocean stratification relies crucially on the

Southern Ocean surface buoyancy flux being dominated by approximately fixed freshwater fluxes. This is in contrast with previous idealized modeling studies [e.g., *Nikurashin and Vallis*, 2012; *Wolfe and Cessi*, 2011], in which the control of the Southern Ocean surface buoyancy forcing over the global deep ocean stratification relies on restoring thermal fluxes. This change in the form of the surface buoyancy forcing extends the control of the Southern Ocean surface forcing up to the core of the NADW overturning circulation cell.

In contrast to deep ocean density stratification, however, we find that although North Atlantic surface forcing does not substantially affect the deep ocean stratification, it does strongly influence the global deep ocean temperature and salinity profiles. In other words, the North Atlantic forcing causes temperature and salinity changes which have canceling contributions to the density. The temperature and salinity stratifications are important because they influence the stored heat and solubility of the abyssal waters, thereby affecting the capacity for carbon storage in the ocean.

In this study we used the ocean component of a single comprehensive climate model, and it is possible that other models may exhibit different responses to similar changes in the surface forcing. For example, the response may depend on the choice of parameterization scheme for unresolved mesoscale eddies [e.g., *Munday et al.*, 2013] and gravity currents [e.g., *Legg et al.*, 2009]. Running CCSM3.5 at an eddy-permitting resolution, *Bryan et al.* [2014] found that the simulated Southern Ocean processes are substantially different than a standard-resolution simulation. The parametrization of diapycnal mixing induced by tidally generated internal waves may also need to be modified to accurately simulate the LGM ocean [*Green et al.*, 2009]. Furthermore, it should also be noted that we are unable to isolate the influence of the Southern Ocean surface wind forcing in the model as it is varied together with the surface buoyancy forcing.

In conclusion, these results suggest that Southern Ocean surface freshwater forcing is largely responsible for the global deep ocean stratification differences between the LGM and PI climates. Considering the influence of deep ocean stratification on CO_2 outgassing [e.g., *Bouttes et al.*, 2009; *Adkins*, 2013], this implies that Southern Ocean surface freshwater forcing plays a central role in glacial-interglacial changes in atmospheric CO_2 concentration. It also implies that Southern Ocean surface freshwater forcing may have a strong influence on the deep ocean stratification and CO_2 storage in future climate change scenarios.

Acknowledgments
This work was supported by National Science Foundation grant OCE-1357078 and OCE-1538702. Without implying their endorsement, we thank Till Wagner, Shang-Ping Xie, Paola Cessi, Maxim Nikurashin, and Tim Merlis for their helpful comments and discussions. We are also grateful to Frank Bryan and David Bailey for technical help with the CESM model setup. Files related to the setup of the CESM simulations, as well as processed model output, are available at http://eisenman.ucsd.edu/code.html. Unprocessed model output is available by request from the corresponding author.

References

Abernathey, R., J. Marshall, and D. Ferreira (2011), The dependence of Southern Ocean meridional overturning on wind stress, *J. Phys. Oceanogr.*, *41*(12), 2261–2278.

Adkins, J. F. (2013), The role of deep ocean circulation in setting glacial climates, *Paleoceanography*, *28*, 539–561, doi:10.1002/palo.20046.

Anderson, R. F., S. Ali, L. I. Bradtmiller, S. H. H. Nielsen, M. Q. Fleisher, B. E. Anderson, and L. H. Burckle (2009), Wind-driven upwelling in the Southern Ocean and the deglacial rise in atmospheric CO_2, *Science*, *323*(5920), 1443–1448.

Bouttes, N., D. Roche, and D. Paillard (2009), Impact of strong deep ocean stratification on the glacial carbon cycle, *Paleoceanography*, *24*, PA3203, doi:10.1029/2008PA001707.

Brady, E. C., B. L. Otto-Bliesner, J. E. Kay, and N. Rosenbloom (2013), Sensitivity to glacial forcing in the CCSM4, *J. Clim.*, *26*(6), 1901–1925.

Bryan, F. O., P. R. Gent, and R. Tomas (2014), Can Southern Ocean eddy effects be parameterized in climate models?, *J. Clim.*, *27*(1), 411–425.

Cerovecki, I., L. D. Talley, and M. R. Mazloff (2011), A comparison of Southern Ocean air-sea buoyancy flux from an ocean state estimate with five other products, *J. Clim.*, *24*(24), 6283–6306.

Clark, P. U., A. S. Dyke, J. D. Shakun, A. E. Carlson, J. Clark, B. Wohlfarth, J. X. Mitrovica, S. W. Hostetler, and A. M. McCabe (2009), The Last Glacial Maximum, *Science*, *325*(5941), 710–714.

Fučkar, N. S., and G. K. Vallis (2007), Interhemispheric influence of surface buoyancy conditions on a circumpolar current, *Geophys. Res. Lett.*, *34*, L14605, doi:10.1029/2007GL030379.

Gent, P. R., and G. Danabasoglu (2011), Response to increasing Southern Hemisphere winds in CCSM4, *J. Clim.*, *24*(19), 4992–4998.

Gent, P. R., G. Danabasoglu, L. J. Donner, M. M. Holland, E. C. Hunke, S. R. Jayne, D. M. Lawrence, R. B. Neale, P. J. Rasch, and M. Vertenstein (2011), The community climate system model version 4, *J. Clim.*, *24*(19), 4973–4991.

Green, J. A., C. L. Green, G. R. Bigg, T. Rippeth, J. D. Scourse, and K. Uehara (2009), Tidal mixing and the meridional overturning circulation from the Last Glacial Maximum, *Geophys. Res. Lett.*, *36*, L15603, doi:10.1029/2009GL039309.

Griffies, S. M., A. Biastoch, C. Böning, F. Bryan, G. Danabasoglu, E. P. Chassignet, M. H. England, R. Gerdes, H. Haak, and Hallberg R. W. (2009), Coordinated ocean-ice reference experiments (COREs), *Ocean Modell.*, *26*(1), 1–46.

Haney, R. L. (1971), Surface thermal boundary condition for ocean circulation models, *J. Phys. Oceanogr.*, *1*(4), 241–248.

Kunze, E., E. Firing, J. M. Hummon, T. K. Chereskin, and A. M. Thurnherr (2006), Global abyssal mixing inferred from lowered ADCP shear and CTD strain profiles, *J. Phys. Oceanogr.*, *36*(8), 1553–1576.

Legg, S., T. Ezer, L. Jackson, B. P. Briegleb, G. Danabasoglu, W. G. Large, W. Wu, Y. Chang, T. M. Ozgokmen, and H. Peters (2009), Improving oceanic overflow representation in climate models: The gravity current entrainment climate process team, *Bull. Am. Meteorol. Soc.*, *90*, 657–670.

Lozier, M. S. (2012), Overturning in the North Atlantic, *Annu. Rev. Mar. Sci.*, *4*, 291–315.

Marshall, J., and K. Speer (2012), Closure of the meridional overturning circulation through Southern Ocean upwelling, *Nat. Geosci.*, *5*(3), 171–180.

Mashayek, A., R. Ferrari, M. Nikurashin, and W. Peltier (2015), Influence of enhanced abyssal diapycnal mixing on stratification and the ocean overturning circulation, *J. Phys. Oceanogr.*, *45*(10), 2580–2597.

Munday, D. R., H. L. Johnson, and D. P. Marshall (2013), Eddy saturation of equilibrated circumpolar currents, *J. Phys. Oceanogr.*, *43*(3), 507–532.
Munk, W., and C. Wunsch (1998), Abyssal recipes II: Energetics of tidal and wind mixing, *Deep Sea Res.*, *45*, 1977–2010.
Munk, W. H. (1966), Abyssal recipes, *Deep Sea Res.*, *13*, 707–730, Elsevier.
Nikurashin, M., and G. Vallis (2011), A theory of deep stratification and overturning circulation in the ocean, *J. Phys. Oceanogr.*, *41*(3), 485–502.
Nikurashin, M., and G. Vallis (2012), A theory of the interhemispheric meridional overturning circulation and associated stratification, *J. Phys. Oceanogr.*, *42*(10), 1652–1667.
Sarmiento, J. L., and J. R. Toggweiler (1984), A new model for the role of the oceans in determining atmospheric pCO_2, *Nature*, *308*(5960), 621–624.
Sigman, D. M., M. P. Hain, and G. H. Haug (2010), The polar ocean and glacial cycles in atmospheric CO_2 concentration, *Nature*, *466*(7302), 47–55.
Stewart, A. L., R. Ferrari, and A. F. Thompson (2014), On the importance of surface forcing in conceptual models of the deep ocean, *J. Phys. Oceanogr.*, *44*(3), 891–899.
Talley, L. D. (2013), Closure of the global overturning circulation through the Indian, Pacific, and Southern Oceans: Schematics and transports, *Oceanography*, *26*(1), 80–97.
Wolfe, C. L., and P. Cessi (2010), What sets the strength of the middepth stratification and overturning circulation in eddying ocean models?, *J. Phys. Oceanogr.*, *40*(7), 1520–1538.
Wolfe, C. L., and P. Cessi (2011), The adiabatic pole-to-pole overturning circulation, *J. Phys. Oceanogr.*, *41*(9), 1795–1810.

Supporting Information for "The influence of Southern Ocean surface buoyancy forcing on glacial-interglacial changes in the global deep ocean stratification"

Shantong Sun,[1] Ian Eisenman,[1] and Andrew L. Stewart [2]

[1]Scripps Institution of Oceanography, University of California, San Diego, La Jolla, USA
[2]Department of Atmospheric and Oceanic Sciences, University of California, Los Angeles, USA

Contents of this file

1. Text S1 to S3
2. Table S1
3. Figures S1 to S10

Introduction

This Supporting Information comprises three sections of text, one table, and ten figures. In Text S1, the CESM simulation set-up is described in detail. In Text S2, we present further analysis of the deep ocean stratification and discuss the issue of model equilibration. In Text S3, we derive the conceptual model used in the main text.

Text S1. CESM setup

We run CESM version 1.1.2 using a configuration in which only the ocean is active. The ocean component of CESM is the Parallel Ocean Program version 2 (POP2) [*Danabasoglu et al.*, 2012], which has 60 vertical levels ranging from 10m at the surface to 250m at the ocean bottom. We use the CESM "f09_g16" grid, which has a horizontal resolution of nominally 1° with the north pole of the ocean grid displaced to Greenland. This is the same grid configuration that was used in the coupled PI simulation [*Gent et al.*, 2011] and the coupled LGM simulations [*Brady et al.*, 2013], from which the forcing in this study is derived. The coupled simulations have a resolution for the land and atmosphere components of $1.9° \times 2.5°$ and the same resolution for the sea ice component as for the ocean.

The Gent-McWilliams (GM) parameterization [*Gent and Mcwilliams*, 1990] is used to represent the unresolved mesoscale eddies. A GM coefficient is adopted that varies proportional to the local density stratification. This coefficient varies in the horizontal directions and decays with depth, mimicking the decay of eddy activity with depth [*Gent and Danabasoglu*, 2011; *Gent*, 2016]. This allows the model simulations to compare more favorably with observations than models that use a constant diffusivity [*Danabasoglu and Marshall*, 2007], and it enables the model to simulate a response to perturbations in the surface forcing that is comparable to simulations run at much higher resolutions [*Gent and Danabasoglu*, 2011; *Gent*, 2016].

The forcing for each ocean-only simulation is constructed from the coupled model output as a series of repeating 30-year cycles using simulations years 1050-1079 of the coupled PI simulation and 1870-1899 of the coupled LGM simulation. Atmospheric forcings including precipitation, solar radiation, surface winds speed, atmospheric pressure, and atmospheric humidity are taken from output reported by the CCSM4 coupler and have 3-hr temporal resolution. Fluxes across the atmosphere-ocean interface, including evaporation, wind stress, upward longwave radiation, latent heat flux, and sensible heat flux, are calculated in the ocean-only runs based on the simulated ocean state and the specified atmospheric state. For ice-related forcing including sea ice concentration (i.e., fraction of grid box covered by ice) and heat flux between the ice and the ocean, we use daily-mean

Corresponding author: Shantong Sun, shantong@ucsd.edu

data reported by the CCSM4 sea ice component (CICE). For other ice-related forcing including freshwater flux, ice/ocean stress, and salt flux, daily output is not available so we use monthly-mean data reported by CICE. For river runoff and glacial runoff we used monthly-mean data reported by the CCSM4 land component (CLM4).

In order to obtain better agreement between the coupled runs and the ocean-only runs, a process called "diddling" is performed on all monthly-mean data. This allows the monthly-mean values to be preserved when the model linearly interpolates between values at the midpoint of each month. Details are given in *Killworth* [1996].

The sea level was about 100m lower at the LGM than today due to the presence of larger high-latitude ice sheets. This gives rise to slightly different coastlines at the LGM, which is accounted for in the coupled CCSM4 LGM simulation. In order to isolate the influence of surface forcing alone, in the present study we use modern ocean bathymetry in the LGM and Test simulations, as in the PI simulation. As a result, some ocean regions in the ocean-only simulations are land in the coupled LGM simulation that is used to generate the forcing fields. If these areas are not treated appropriately, they can lead to the generation of extremely cold surface water due to the direct contact with the cold terrestrial atmosphere in locations where sea ice would have formed if the sea ice model were active (this is exacerbated by the fact that the surface air in some of these locations is hundreds of meters above the sea level at the surface of the ice sheet in the coupled LGM simulation). To address this issue, both the sea ice concentration and atmospheric forcing need to be adjusted when we apply LGM forcing in locations that are ocean in the PI bathymetry but land in the coupled LGM simulation. We adjust the surface air temperature and potential temperature in these locations by assuming a constant lapse rate of $-6.5^{\circ}\mathrm{C}/\mathrm{km}$ to account for the change of surface geopotential height between the coupled LGM and coupled PI runs. The surface atmospheric pressure is adjusted by assuming exponential decay with height, $p = p_0 \exp(-z/H)$, where $H = 7.6$km is the scale height. The sea ice concentration (c) in these grid cells is prescribed based on the surface air temperature (T) as $c = 1/2 \tanh[(T - T_0)/T_0] + 1/2$, where $T_0 = -2^{\circ}$C. This is motivated by the observation that in the coupled simulations, most ocean locations with surface air temperature below -5°C have ice concentrations close to 100%, and most ocean locations with surface air temperature above 0°C have ice concentrations close to 0%. All fluxes between the ice and ocean in these grid cells are set to zero, including the freshwater flux, salt flux, and momentum flux.

All forcing fields in the ocean-only simulations are from the coupled simulations as specified in Section 2 of the main text, with two exceptions. First, all three ocean-only simulations use the same run-off forcing, which is derived from the coupled PI run. Second, for the weak restoring of surface salinity, which is included in the ocean-only model as described in *Griffies et al.* [2009], the Test run uses salinity restoring field derived from the coupled PI run at all locations, including the Southern Ocean. This simplification appears to have only a small influence on the Test run: the difference between the LGM and Test freshwater fluxes associated with the weak restoring of surface salinity in most Southern Ocean locations is less than 10% of the difference between the LGM and PI runs (not shown), and the surface buoyancy forcing profiles in the Southern Ocean are nearly indistinguishable between the LGM and Test runs (see Figure 1 in the main text).

The surface temperature and salinity for the three ocean-only runs are shown in Figs. S1 and S2. In general, the surface salinity is less constrained by the forcing than the surface temperature. This is expected because the freshwater flux more closely resembles a fixed flux, while the heat flux more closely resembles a relaxation boundary condition [*Haney*, 1971] that tends to fix the surface temperature. Under fixed flux boundary conditions, the actual value of surface salinity is strongly influenced by salt fluxes within the ocean.

Text S2. Details of the deep ocean stratification and model equilibration

The zonal mean stratification in the Atlantic Ocean is shown in Figure S3, with the basin-average stratification profile given in Figure S4 for the South Atlantic, South Pacific, and Indian

Table S1. Durations of model simulations and trends of global volume-average temperature, ideal age, and AMOC max calculated over the last 120 years of each run.

Run Name	PI	Test	LGM
Surface forcing	PI	PI&LGM	LGM
Duration (years)	510	1020	1440
Temperature trend ($^\circ$C/century)	-0.046	-0.048	-0.053
Ideal Age trend (year/century)	16.8	8.8	9.6
AMOC max trend (Sv/Century)	-0.28	-0.16	-0.64

Oceans, and in Figure S5 for the North Atlantic, North Pacific, and Southern Oceans. In every ocean basin the Test run approximately reproduces the LGM deep ocean stratification below 2000m. The deep stratification in the Atlantic Ocean is stronger than in the other ocean basins, which is likely due to the presence of the North Atlantic Deep Water (NADW).

Figure S6 shows the change in the stratification between the last two 30-year periods in the Atlantic Ocean as an indication of the level of equilibration in the simulations. The PI run has a similar trend to the Test run, while the LGM run has a trend that is approximately 3 times larger. The magnitude of the deep ocean stratification changes from one 30-year period to the next (Figure S6) are approximately 100 times smaller than the differences between the three simulations (Figure S3).

Text S3. Conceptual model

S3.i: Derivation of the conceptual model

The derivation of the conceptual model follows *Nikurashin and Vallis* [2011] and *Nikurashin and Vallis* [2012]; see these studies for further details. The model takes a zonally-averaged view of the global stratification and overturning circulation, which are described by the zonal-mean buoyancy $b^* \equiv -g(\rho - \rho_0)/\rho_0$ and overturning circulation streamfunction $\psi(y, z)$. Here we use ψ to describe the zonally integrated circulation rather than the zonal-mean circulation, i.e., ψ has units of m^3/s rather than m^2/s as in *Nikurashin and Vallis* [2012]. The ocean is approximated to consist of a single basin (e.g., the Atlantic) of meridional length L_y and zonal length L_x, which is connected to a re-entrant zonal channel at the southern boundary (resembling the Southern Ocean). This configuration is sketched in Figure 2c in the main text. In the basin the isopycnals are assumed to be flat, so we define $b(z) \equiv b^*(y, z)$ for all $y > 0$, while in the channel ($y < 0$) the isopycnals are assumed to have a constant isopycnal slope s. The surface of the channel is subject to a fixed downward buoyancy flux $B(y)$, and the formation of NADW at the northern end of the basin is represented by $\psi^*(z) \equiv \psi(L_y, z)$. The flow in the channel is assumed to be adiabatic, while the basin is subject to a constant diapycnal diffusivity κ.

Following *Nikurashin and Vallis* [2012], volume conservation implies that at a given depth, the change in the overturning streamfunction across the basin is equal to the net upwelling driven by diapycnal diffusion within the basin,

$$\psi^*(z) - \psi(0, z) = \frac{\kappa\, L_y\, L_x}{N^2} \frac{\partial}{\partial z} N^2(z), \tag{S1}$$

where $y = 0$ represents the northern boundary of the Southern Ocean (Figure 2c). Here $N^2 \equiv \partial b/\partial z$ is the Brunt-Väisälä frequency, which is a measure of the ocean density stratification. For isopycnals that outcrop in the Southern Ocean, the overturning streamfunction at the base of the

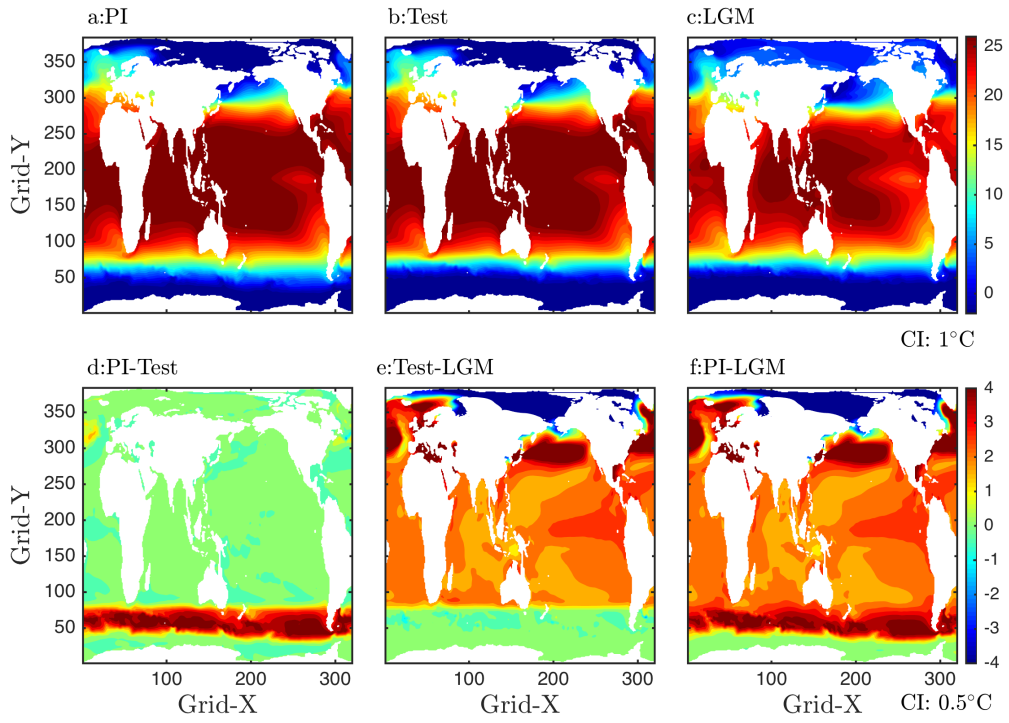

Figure S1. Long-term mean surface potential temperature (° C) in the three model runs and the differences between them. The fields are plotted here on the coordinates of the ocean model grid, which has the North Pole displaced to Greenland [*Danabasoglu et al.*, 2006].

mixed layer ($z = 0$) can be related to the surface buoyancy forcing by

$$\psi(y, 0) = \frac{L_x\, B(y)}{\partial b/\partial y} \tag{S2}$$

for $y < 0$ [cf. *Marshall and Radko*, 2003]. Since the overturning circulation is assumed to be adiabatic in the Southern Ocean, the value of the streamfunction at the base of the mixed layer ($z = 0$) must match the value at the northern edge of the channel ($y = 0$) along the same isopycnal. For constant isopycnal slope s in the Southern Ocean, this implies

$$\psi(-z/s, 0) = \psi(0, z). \tag{S3}$$

Combining equation (S1), (S2), and (S3), we obtain

$$\frac{\kappa\, L_y\, L_x}{N^2(z)} \frac{\partial}{\partial z} N^2(z) = \psi^*(z) + L_x \frac{B(-z/s)}{s\, N^2(z)}, \tag{S4}$$

which is equivalent to equation (2) in the main text.

Isopycnals in Region 3 outcrop only in the Southern Ocean, and ψ^* is zero at the northern boundary. Therefore equation (S4) reduces to

$$\kappa\, s\, L_y \frac{\partial}{\partial z} N^2(z) = B(-z/s), \tag{S5}$$

which is equivalent to equation (3) in the main text. Assuming that N^2 is negligibly small at the bottom boundary $z = z_{bot}$ (see Figure 3a in the main text), integration of equation (S5) shows that

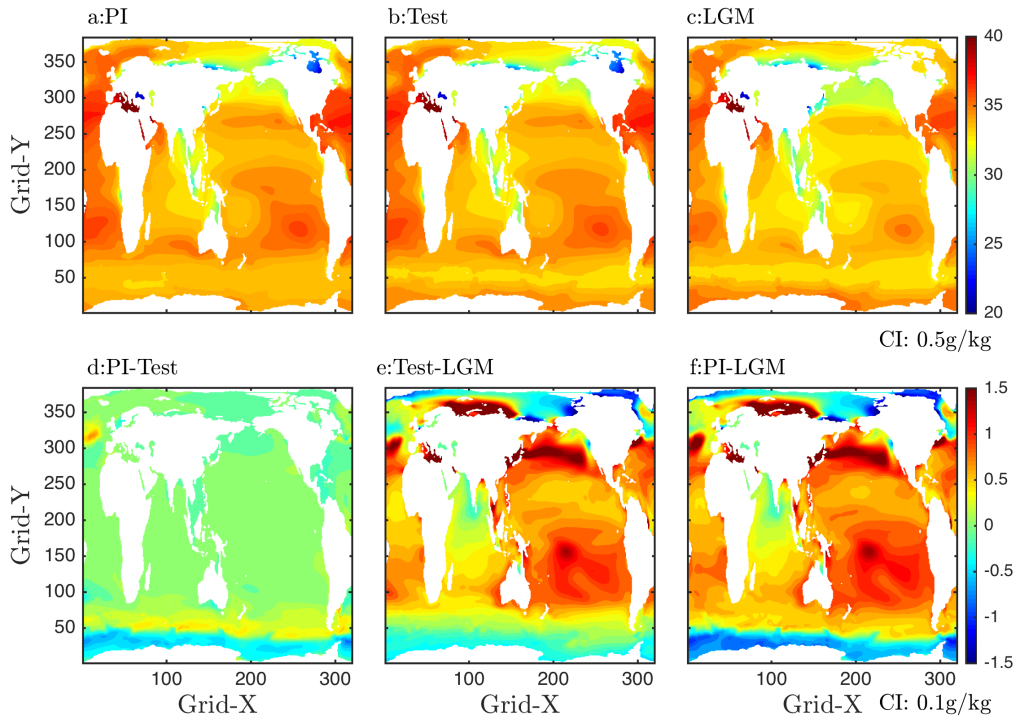

Figure S2. Long-term mean surface salinity (g/kg) in the three model runs and the differences between them. Coordinates are as in Figure S1.

the stratification in Region 3 is determined by the surface buoyancy forcing in the Southern Ocean only as long as B is specified:

$$N^2(z) = \int_{z_{bot}}^{z} \frac{B(-z'/s)}{\kappa\, s\, L_y} dz'. \tag{S6}$$

However, if the surface buoyancy forcing takes the form of a relaxation boundary condition, $B(y) = r\,[\,b_s(y) - b^*(y,0)\,]$ with r the relaxation coefficient, b_s the specified surface buoyancy, and $b^*(y,0)$ the buoyancy at the surface of the Southern Ocean, then the buoyancy $b(z)$ appears on both sides of equation (S6), so this equation no longer directly indicates what determines the stratification. In this case, equation (S5) becomes

$$\kappa\, s\, L_y \frac{\partial}{\partial z} N^2(z) + r\, b(z) = r\, b_s(-z/s), \tag{S7}$$

where we have used $b^*(y,0) = b^*(-z/s,0) = b(z)$, i.e., the buoyancy in the basin is equal to the buoyancy at the surface of the Southern Ocean along the same isopycnal. Since $N^2 \equiv \partial b/\partial z$, equation (S7) is a second-order ordinary differential equation for $b(z)$. In this case, the abyssal stratification is affected by the upper boundary condition for b, and so it is subject to at least slight inter-hemispheric influences as expected from *Fučkar and Vallis* [2007].

In Region 2, where ψ^* does not vanish, we consider the difference between the stratifications in the LGM and Test runs, which can be derived from equation (S4) as

$$\kappa\, L_y\, L_x \frac{\partial}{\partial z}\left(N^2_{\mathrm{LGM}}(z) - N^2_{\mathrm{Test}}(z)\right) = \left(N^2_{\mathrm{LGM}}(z)\psi^*_{\mathrm{LGM}}(z) - N^2_{\mathrm{Test}}(z)\psi^*_{\mathrm{Test}}(z)\right) + \frac{L_x}{s}\left(B_{\mathrm{LGM}}(-z/s) - B_{\mathrm{Test}}(-z/s)\right), \tag{S8}$$

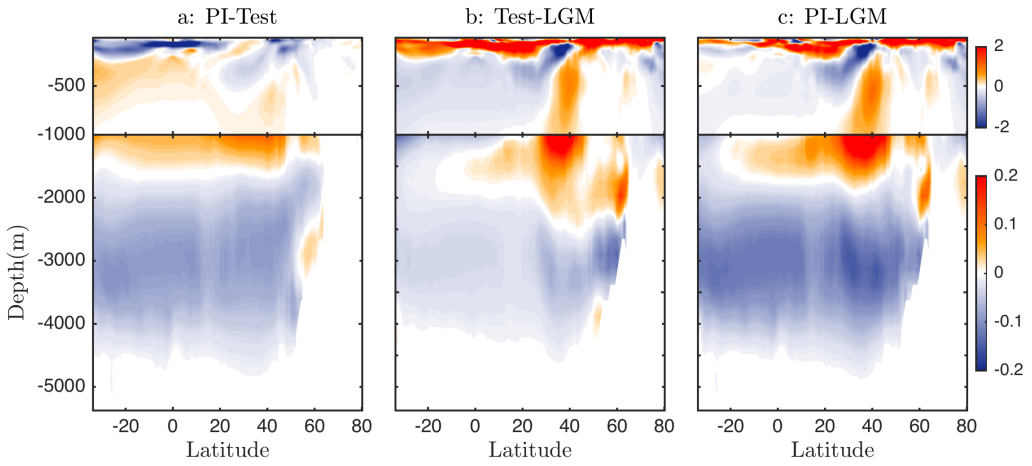

Figure S3. Comparison of the zonal-mean stratification in the Atlantic Ocean between the three model runs (N^2, in units of 10^{-5} s^{-2}). Note that the magnitude of the stratification difference in panel b below about 2000m is 10 times smaller than that in panels a and c.

where the subscripts indicate the simulation name. Since both the LGM and Test simulations are subject to the same approximately fixed LGM surface forcing in the Southern Ocean, we approximate the last term in equation (S8) to be negligibly small (see Figure 1 in the main text), and equation (S8) becomes

$$\begin{aligned}
\kappa\, L_y L_x \frac{\partial}{\partial z}\left(N^2_{\rm LGM}(z) - N^2_{\rm Test}(z)\right) &= N^2_{\rm LGM}(z)\psi^*_{\rm LGM}(z) - N^2_{\rm Test}(z)\psi^*_{\rm Test}(z) \\
&= N^2_{\rm LGM}(z)\left(\psi^*_{\rm LGM}(z) - \psi^*_{\rm Test}(z)\right) + \\
&\qquad \psi^*_{\rm Test}(z)\left(N^2_{\rm LGM}(z) - N^2_{\rm Test}(z)\right) \\
&= N^2_{\rm LGM}(z)\Delta\psi^* + \psi^*_{\rm Test}\Delta N^2 \\
&= N^2_{\rm LGM}(z)\Delta\psi^*\left(1 + \frac{\psi^*_{\rm Test}\Delta N^2}{\Delta\psi^* N^2}\right). \qquad \text{(S9)}
\end{aligned}$$

At the depth of isopycnal surface ρ_2 that separates the upper and lower overturning cells, defined here as z_0, $N^2_{\rm LGM} \approx N^2_{\rm Test} \gg \Delta N^2$ and $\psi^*_{\rm Test} \sim \psi^*_{\rm LGM} \sim \Delta\psi^* \sim 0$, as discussed above. Hence $\frac{\psi^*_{\rm Test}\Delta N^2}{\Delta\psi^* N^2} \ll 1$ and equation (S9) can be approximately written near $z = z_0$ as

$$\kappa\, L_y\, L_x \frac{\partial}{\partial z}\Delta N^2(z) \approx N^2_{\rm LGM}(z)\Delta\psi^*(z), \qquad \text{(S10)}$$

where $\Delta N^2 \equiv N^2_{\rm LGM} - N^2_{\rm Test}$ and $\Delta\psi^* \equiv \psi^*_{\rm LGM} - \psi^*_{\rm Test}$. Using a realistic Atlantic area of $L_x\, L_y = 8 \times 10^{13}$m^2, diapycnal diffusivity of $\kappa = 1 \times 10^{-4}$ m^2/s, and Region 2 approximate depth range of $\delta z = 1000$m, this implies that the NADW streamfunction must differ between the LGM and Test runs by $\Delta\psi^* \approx 8\,$Sv in order to produce an order-one fractional change in the vertical change of the stratification over the depth of Region 2. Given the small change in NADW of about 2 Sv between the LGM and Test simulations, we suggest that this explains why the change in stratification across the depth range of Region 2 (approximately 2km to 3km) is similar in the LGM and Test simulations (red and green lines in Figure 3a of the main text).

Note that in Region 1, the influence from the surface wind-driven circulation is non-negligible, so the assumption adopted here of flat isopycnals in the basin is not applicable.

An important caveat is that this conceptual model is only used in order to achieve a qualitative understanding of the influence of the Southern Ocean surface forcing on the abyssal and mid-depth

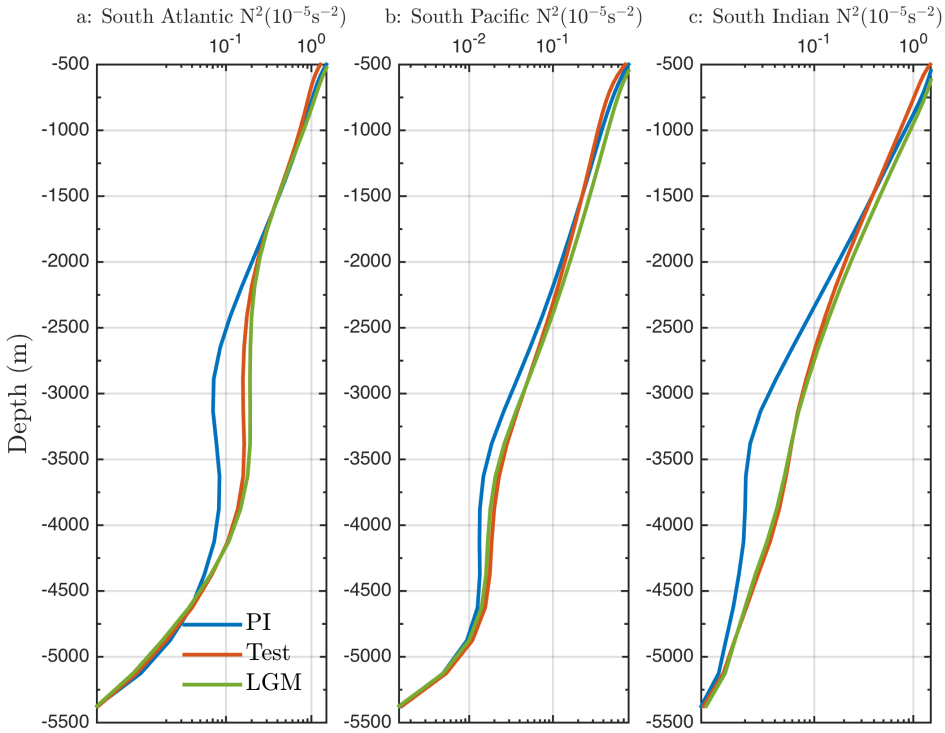

Figure S4. Basin-averaged stratification in the South Atlantic, South Pacific, and South Indian Oceans (N^2, in units of 10^{-5} s^{-2}).

stratification. This model should not be expected to quantitatively reproduce the stratification profiles shown in Figure S4 and S5. For example, the stratification in the Atlantic is clearly different from the other basins, which is not accounted for in this conceptual model. Furthermore, the assumption of an adiabatic Southern Ocean circulation in our conceptual model is not strictly justified. This can be seen in Figure S7, which shows the residual overturning circulation streamfunction in the Southern Ocean for the three model runs, calculated in σ_2 coordinates. A diabatic component to the circulation south of 50°S is readily discernible. This enhanced diapycnal flow in the Southern Ocean is mainly associated with the deep mixed layer inside the subpolar gyre. Away from the subpolar gyre region, the residual overturning circulation streamfunction approximately follows isopycnals, i.e., the adiabatic assumption is approximately satisfied.

S3.ii: Non-constant isopycnal slope

In the analysis above, we assumed a constant isopycnal slope in the Southern Ocean for simplicity, and we concluded that the NADW streamfunction would need to differ considerably between the LGM and Test runs to produce a substantial change in the stratification of Region 2. Here we show this conclusion still holds if we relax the assumption of constant isopycnal slope in the Southern Ocean to allow the slope to vary between different isopycnals. Note that this analysis will focus on the Southern Ocean region, whereas the analysis in Section S3.i focused on the basin north of the Southern Ocean.

Following *Nikurashin and Vallis* [2011], the residual overturning circulation streamfunction in the Southern Ocean can be written as

$$\psi = \psi^{+} + \psi^{\#}. \tag{S11}$$

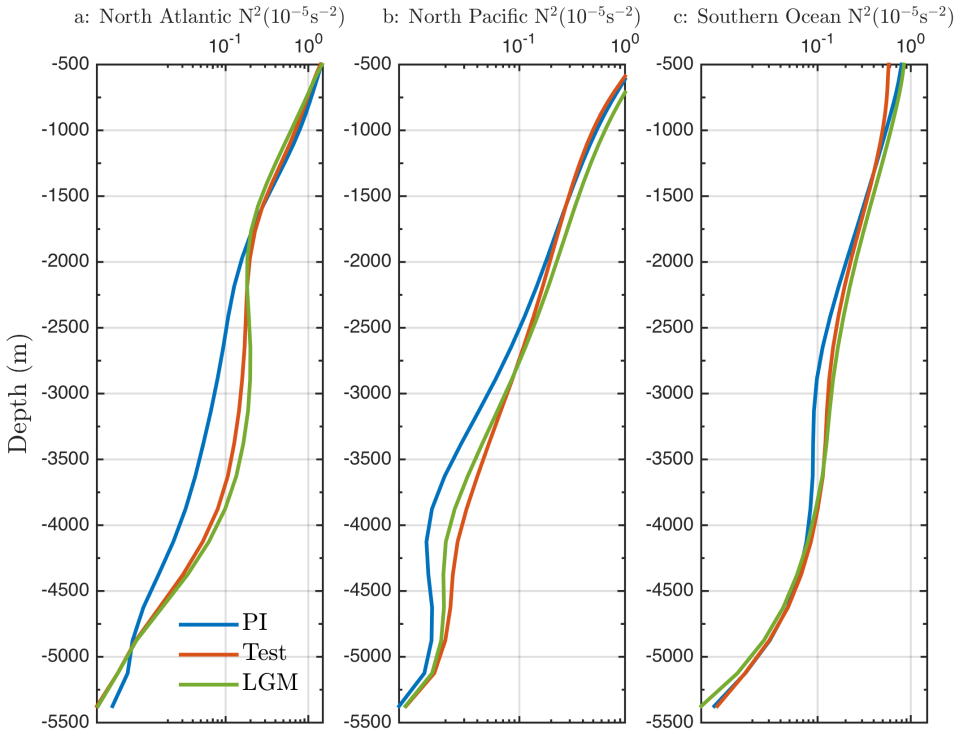

Figure S5. Basin-averaged stratification in the North Atlantic, North Pacific, and Southern Oceans (N^2, in units of 10^{-5} s^{-2}).

Here, ψ^+ represents the contribution from mean flow and is given by the surface Ekman transport,

$$\psi^+ = -\frac{\tau_0 \, L_x}{f_0 \rho_0}, \tag{S12}$$

and $\psi^\#$ is the eddy-driven overturning circulation streamfunction which can be expressed as

$$\psi^\# = L_x \, K_{\rm GM} \, s \tag{S13}$$

based on the Gent-McWilliams (GM) parameterization of mesoscale eddies. Here $K_{\rm GM}$ is the GM thickness diffusivity which is a function of the local stratification in our ocean-only CESM simulations. We assume for simplicity that the surface wind stress forcing (τ_0) and Coriolis parameter (f_0) are constant, which implies that ψ^+ is constant across the Southern Ocean and all Eulerian-mean vertical motions occur in the southern and northern boundary of the Southern Ocean. This simplification is also made in *Nikurashin and Vallis* [2011] for qualitative discussions.

In the ocean-only CESM simulations, both the GM thickness diffusivity $K_{\rm GM}$ and isopycnal slope s vary somewhat in the Southern Ocean (Figure S9 and S10), and they combine together to support the southward NADW transport into the Southern Ocean as in *Abernathey et al.* [2011], i.e., both $K_{\rm GM}$ and s vary to account for the vertical change of ψ at the northern boundary of the Southern Ocean. Here, for simplicity, we only allow s to vary but keep $K_{\rm GM}$ constant, as in previous idealized modeling studies [e.g., *Wolfe and Cessi*, 2011].

Furthermore, we assume the circulation in the Southern Ocean to be adiabatic, i.e., the residual overturning circulation streamfunction ψ is constant along each individual isopycnal surface. Hence the assumption of a constant ψ^+ implies that the eddy-driven overturning circulation streamfunction $\psi^\#$ must also be constant along each isopycnal surface.

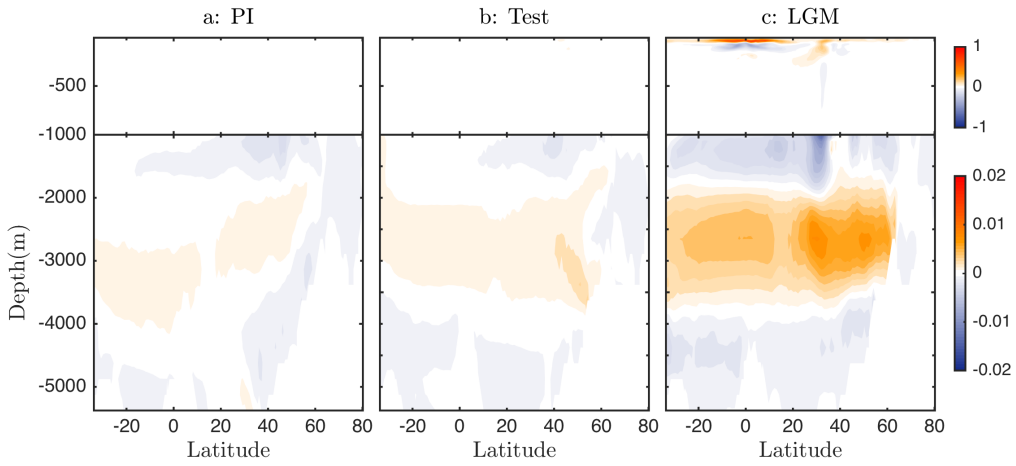

Figure S6. Change of the zonal-mean stratification in the Atlantic Ocean between the last two 30-year cycles (N^2, in units of 10^{-5} s^{-2}). Note that the magnitude of the stratification change in the deep ocean is of order 0.001×10^{-5} s^{-2}, which is 100 times smaller than in Figure S3.

Consider the residual overturning circulation on two isopycnals, ρ_2 and ρ_*, where ρ_2 is indicated in Figure 2c as the isopycnal that separates the abyssal overturning circulation from the region above, and ρ_* can be any isopycnal between ρ_1 and ρ_2. In the Southern Ocean, the southward flux of NADW ($\psi_{\rm NADW}$) between ρ_2 and ρ_* has to be balanced by the vertical change in the eddy-driven overturning circulation streamfunction since the Eulerian-mean overturning circulation (ψ^+) has been assumed to be constant,

$$\psi_{\rm NADW} = \psi_* - \psi_2 = \psi_*^\# - \psi_2^\#. \tag{S14}$$

Here, ψ_* and ψ_2 are the residual overturning circulation streamfunction on isopycnal surface ρ_* and ρ_2, and $\psi_*^\#$ and $\psi_2^\#$ are the eddy-driven overturning circulation streamfunction on isopycnal surfaces ρ_* and ρ_2. Combining equation (S13) and (S14), we have

$$\psi_{\rm NADW} = L_x K_{\rm GM}(s_* - s_2), \tag{S15}$$

where s_* and s_2 are the slopes of isopycnals ρ_* and ρ_2, respectively. At the surface of the Southern Ocean, the upwelled water is transformed to lighter water by the surface buoyancy flux B (which is fixed, i.e., independent of the ocean state), which satisfies

$$\frac{B}{\partial b/\partial y} = \frac{\psi_{\rm NADW}}{L_x}. \tag{S16}$$

In equation (S16), both B and $\partial b/\partial y$ are evaluated at the surface in the Southern Ocean where ρ_* outcrops. The buoyancy gradient $\partial b/\partial y$ can be approximated by

$$\frac{\partial b}{\partial y} \approx -\frac{\rho_* - \rho_2 g}{\rho_0 W} = \frac{g'}{W}, \tag{S17}$$

where $g' \equiv (\rho_* - \rho_2 g)/\rho_0$ and W is the distance between ρ_2 and ρ_* at the ocean surface, i.e.,

$$W = \frac{z_2}{s_2} - \frac{z_*}{s_*}. \tag{S18}$$

Based on our definition of ρ_2,

$$\psi_2 = 0 \text{ and } \mathrm{s_2} = -\frac{\tau_0}{\rho_0 \mathrm{f_0 K_{GM}}} \tag{S19}$$

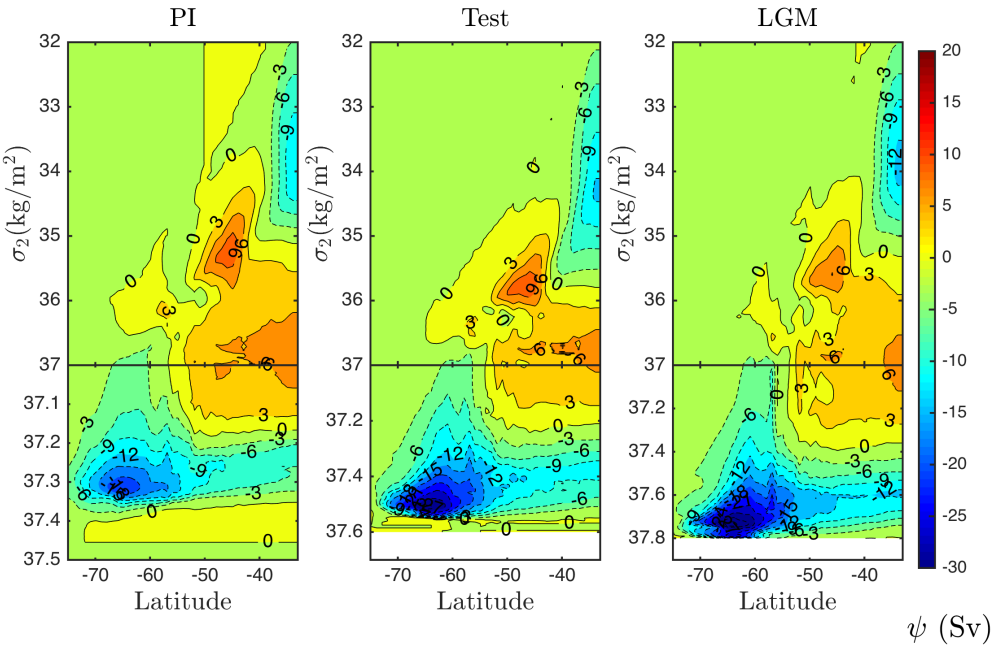

Figure S7. Residual overturning circulation streamfunction in the Southern Ocean (Sv) using σ_2 as the vertical coordinate.

are specified constants.

Combining equation (S16), (S17) and (S18), we obtain

$$\frac{B}{g'}\left(\frac{z_2}{s_2}-\frac{z_*}{s_*}\right)=\frac{\psi_{\mathrm{NADW}}}{L_x}. \tag{S20}$$

Substituting equation (S15) into (S20) leads to

$$\frac{B}{g'}\left[\frac{z_2}{s_2}-\frac{z_*}{s_2+\psi_{\mathrm{NADW}}/(K_{\mathrm{GM}}L_x)}\right]=\frac{\psi_{\mathrm{NADW}}}{L_x}, \tag{S21}$$

from which we can obtain

$$\frac{z_*}{s_2+\psi_{\mathrm{NADW}}/(K_{\mathrm{GM}}L_x)}=\frac{z_2}{s_2}-\frac{\psi_{\mathrm{NADW}}\,g'}{BL_x}. \tag{S22}$$

Therefore, the difference in depth between ρ_* and ρ_2 is

$$z_*-z_2=\underbrace{\frac{z_2}{s_2}\frac{\psi_{\mathrm{NADW}}}{K_{\mathrm{GM}}L_x}}_{\mathrm{I}}-\underbrace{\frac{\psi_{\mathrm{NADW}}\,g'}{BL_x}\left(s_2+\frac{\psi_{\mathrm{NADW}}}{K_{\mathrm{GM}}L_x}\right)}_{\mathrm{II}}. \tag{S23}$$

Here Term I represents the effect of the reduction in the isopycnal slope that supports a positive overturning overturning streamfunction because $s_*-s_2=\psi_{\mathrm{NADW}}/(L_xK_{\mathrm{GM}})$ from equation (S15). Term II represents the contribution from the northward displacement of the outcropping latitude of ρ_* relative to ρ_2 because $(\psi_{\mathrm{NADW}}\,g')/(BL_x)\approx W$ based on equation (S16) and (S17).

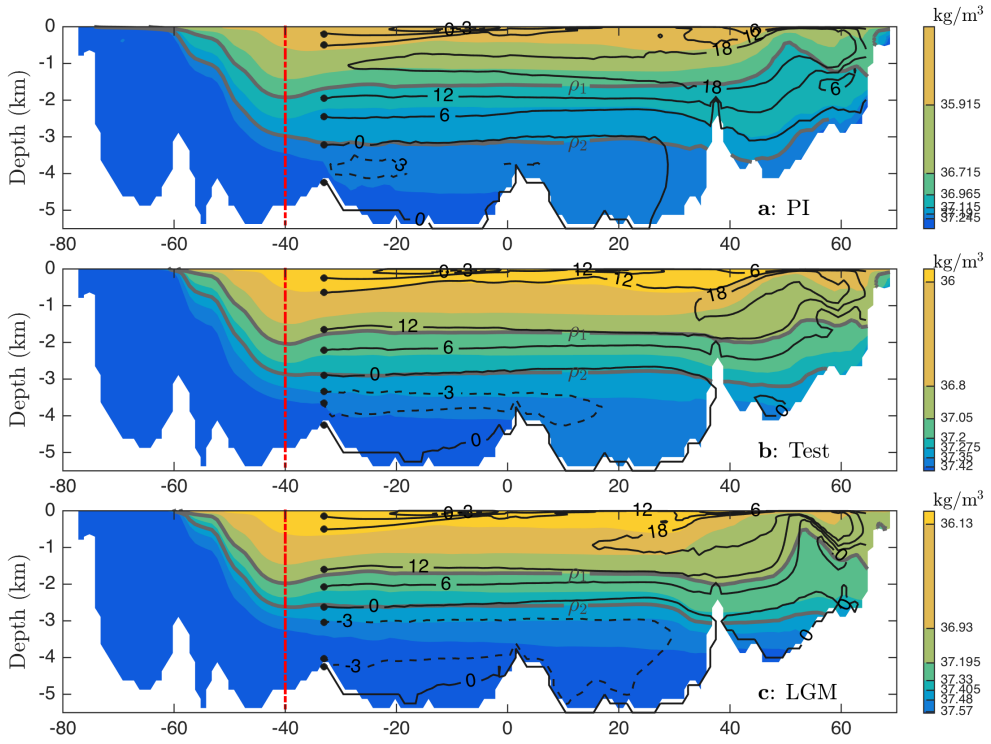

Figure S8. As in Figure 2b in the main text, but including the PI and LGM simulations as well as the Test simulation. (Note that panel b here is equivalent to Figure 2b.)

For typical values in the real ocean:

$$\begin{aligned} \psi_{\mathrm{NADW}} &= 10^7 \mathrm{m}^3/\mathrm{s}, & s_2 &= -10^{-3}, \\ L_x &= 2\times 10^7 \mathrm{m}, & \rho_0 &= 1000 \mathrm{kg/m}^3, \\ K_{\mathrm{GM}} &= 1000 \mathrm{m}^2/\mathrm{s}, & \rho_2 - \rho_* &= 0.2 \mathrm{kg/m}^3, \\ B &= 10^{-8} \mathrm{m}^2/\mathrm{s}^3, & z_2 &= -3000 \mathrm{m}. \end{aligned}$$

Here the value of ρ_* is chosen close to the core of the NADW overturning circulation, where there is maximal change in the isopycnal slope.

We obtain

$$z_* - z_2 = \underbrace{1500m}_{\mathrm{I}} + \underbrace{50m}_{\mathrm{II}}\,. \tag{S24}$$

Clearly, term I dominates over term II in equation (S23). Thus, we have

$$z_* - z_2 \approx \frac{z_2 \psi_{\mathrm{NADW}}}{s_2\, K_{\mathrm{GM}} L_x}. \tag{S25}$$

Inserting equation (S25) into the approximate derivative $N^2 \approx g'/(z_* - z_2)$, the density stratification in Region 2 is

$$N^2 \approx \frac{\Lambda}{\psi_{\mathrm{NADW}}}, \tag{S26}$$

with

$$\Lambda \equiv \frac{g' s_2\, K_{\mathrm{GM}} L_x}{z_2} \tag{S27}$$

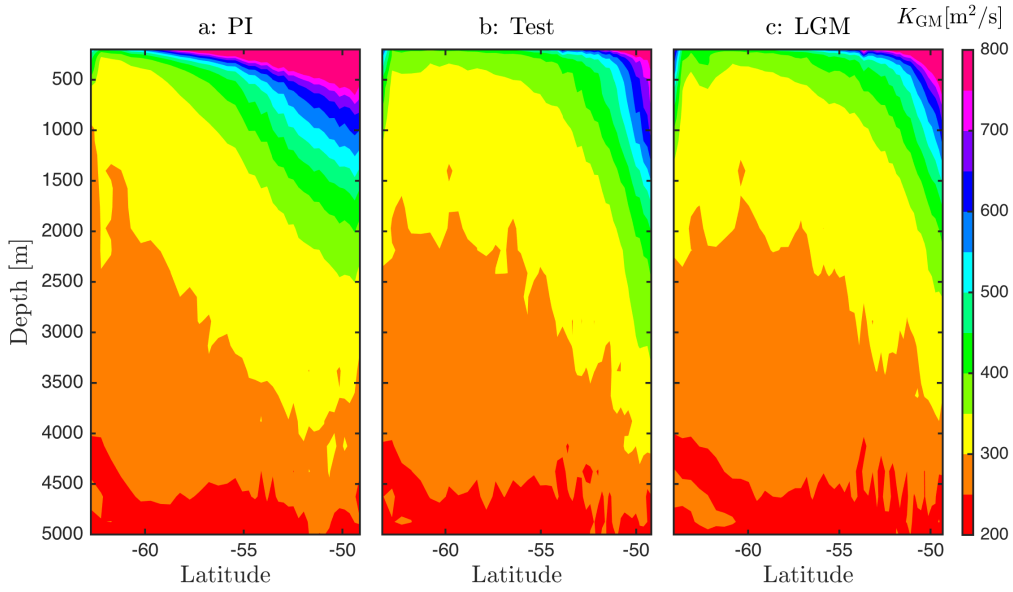

Figure S9. Gent-McWilliams (GM) thickness diffusion coefficient (K_{GM}; units of m^2/s) averaged zonally along barotropic streamlines.

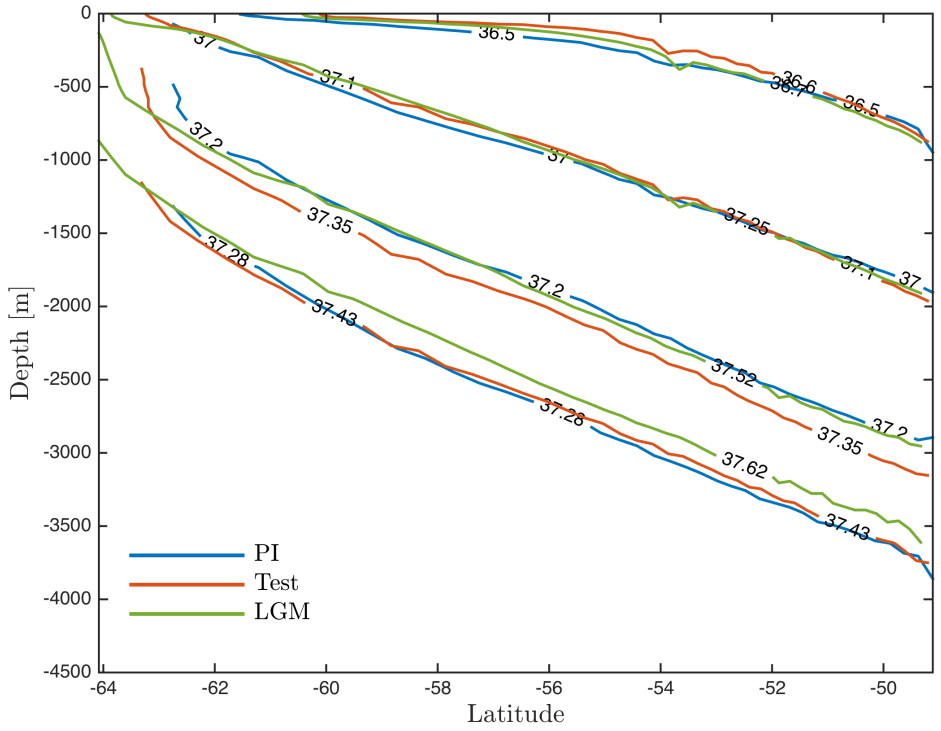

Figure S10. Isopycnal contours of σ_2 (units of kg/m^3) averaged zonally along barotropic streamlines.

being a constant. From equation (S26), we obtain

$$\Delta N^2 \approx -\frac{\Lambda}{\psi^2_{\mathrm{NADW:LGM}}}\Delta\psi_{\mathrm{NADW}}. \tag{S28}$$

Here $\Delta\psi_{\mathrm{NADW}} \equiv \psi_{\mathrm{NADW:LGM}} - \psi_{\mathrm{NADW:Test}}$, where $\psi_{\mathrm{NADW:LGM}}$ and $\psi_{\mathrm{NADW:Test}}$ are the values of ψ_{NADW} in the LGM and Test simulations. Recall that $\Delta N^2 \equiv N^2_{\mathrm{LGM}} - N^2_{\mathrm{Test}}$. To obtain equation (S28), we have used the assumption $\psi_{\mathrm{NADW:LGM}} \approx \psi_{\mathrm{NADW:Test}}$. Combining equation (S26) with (S28) leads to

$$\frac{\Delta N^2}{N^2_{\mathrm{LGM}}} \approx -\frac{\Delta\psi_{\mathrm{NADW}}}{\psi_{\mathrm{NADW:LGM}}}. \tag{S29}$$

Therefore, even when the assumption of constant isopycnal slope is relaxed, an order-one change in NADW transport is still required for the Northern Hemisphere surface forcing alone to cause an order-one change in the density stratification in Region 2. Consistent with the simpler analysis in Section S3.i, we suggest that this explains why the stratification in Region 2 was relatively insensitive to changes in Northern Hemisphere surface forcing.

References

Abernathey, R., J. Marshall, and D. Ferreira (2011), The dependence of Southern Ocean meridional overturning on wind stress, *J. Phys. Oceanogr.*, *41*(12), 2261–2278.

Brady, E. C., B. L. Otto-Bliesner, J. E. Kay, and N. Rosenbloom (2013), Sensitivity to glacial forcing in the CCSM4, *J. Clim.*, *26*(6), 1901–1925.

Danabasoglu, G., and J. Marshall (2007), Effects of vertical variations of thickness diffusivity in an ocean general circulation model, *Ocean Modell.*, *18*(2), 122–141.

Danabasoglu, G., W. G. Large, J. J. Tribbia, P. R. Gent, B. P. Briegleb, and J. C. McWilliams (2006), Diurnal coupling in the tropical oceans of CCSM3, *J. of Clim.*, *19*(11), 2347–2365.

Danabasoglu, G., S. C. Bates, B. P. Briegleb, S. R. Jayne, M. Jochum, W. G. Large, S. Peacock, and S. G. Yeager (2012), The CCSM4 ocean component, *J. Clim.*, *25*(5), 1361–1389.

Fučkar, N. S., and G. K. Vallis (2007), Interhemispheric influence of surface buoyancy conditions on a circumpolar current, *Geophys. Res. Lett.*, *34*(14).

Gent, P. R. (2016), Effects of Southern Hemisphere Wind Changes on the Meridional Overturning Circulation in Ocean Models, *Annu. Rev. Mar. Sci.*, *8*, 79–84.

Gent, P. R., and G. Danabasoglu (2011), Response to increasing Southern Hemisphere winds in CCSM4, *J. Clim.*, *24*(19), 4992–4998.

Gent, P. R., and J. C. Mcwilliams (1990), Isopycnal mixing in ocean circulation models, *J. Phys. Oceanogr.*, *20*(1), 150–155.

Gent, P. R., G. Danabasoglu, L. J. Donner, M. M. Holland, E. C. Hunke, S. R. Jayne, D. M. Lawrence, R. B. Neale, P. J. Rasch, M. Vertenstein, et al. (2011), The community climate system model version 4, *J. Clim.*, *24*(19), 4973–4991.

Griffies, S. M., A. Biastoch, C. Böning, F. Bryan, G. Danabasoglu, E. P. Chassignet, M. H. England, R. Gerdes, H. Haak, R. W. Hallberg, et al. (2009), Coordinated ocean-ice reference experiments (COREs), *Ocean Modell.*, *26*(1), 1–46.

Haney, R. L. (1971), Surface thermal boundary condition for ocean circulation models, *J. Phys. Oceanogr.*, *1*(4), 241–248.

Killworth, P. D. (1996), Time interpolation of forcing fields in ocean models, *J. Phys. Oceanogr.*, *26*(1), 136–143.

Marshall, J., and T. Radko (2003), Residual-mean solutions for the Antarctic Circumpolar Current and its associated overturning circulation, *J. Phys. Oceanogr.*, *33*(11), 2341–2354.

Nikurashin, M., and G. Vallis (2011), A theory of deep stratification and overturning circulation in the ocean, *J. Phys. Oceanogr.*, *41*(3), 485–502.

Nikurashin, M., and G. Vallis (2012), A theory of the interhemispheric meridional overturning circulation and associated stratification, *J. Phys. Oceanogr.*, *42*(10), 1652–1667.

Wolfe, C. L., and P. Cessi (2011), The adiabatic pole-to-pole overturning circulation, *J. Phys. Oceanogr.*, *41*(9), 1795–1810.